Structure and Bonding of the Coordinatively Unsaturated Complexes $[Fe_2(CO)_5(\mu\text{-}PR_2)(\mu\text{-}PR'_2)](Fe{=}Fe)$ (R = R' = Bu^t; R = Ph, R' = Bu^t). Reaction of $Na[Fe_2(\mu\text{-}CO)(CO)_6(\mu\text{-}PR_2)]$ with R'_2PCl (R, R' = Ph, Cy, Me, Bu^t)

Bernhard Walther,*,† Helmut Hartung,*,† Joachim Reinhold,*,‡ Peter G. Jones,§ Carlo Mealli,∥ Hans-C. Böttcher,† Ute Baumeister,† André Krug,† and Andrea Möckel†

Departments of Chemistry, Martin Luther University Halle-Wittenberg, Weinbergweg 16, O-4050 Halle, Germany, University of Leipzig, Talstrasse 35, O-7010 Leipzig, Germany, Technical University Braunschweig, Hagenring 30, W-3300 Braunschweig, Germany, and Istituto per lo Studio della Stereochimica ed Energetica dei Composti di Coordinazione, CNR, Via J. Nardi 39, 50132 Firenze, Italy

Received September 26, 1991

The reaction of anions $[Fe_2(\mu\text{-}CO)(CO)_6(\mu\text{-}PR_2)]^-$ with R'_2PCl gives either the electron-precise bis(phosphido)-bridged diiron hexacarbonyl complexes $[Fe_2(CO)_6(\mu\text{-}PR_2)(\mu\text{-}PR'_2)]$ (R = Ph, R' = Cy (1), Bu^t (3); R = R' = Cy (2); R = Me, R' = Bu^t (4)) or the new electron-deficient diiron pentacarbonyl complex $[Fe_2(CO)_5(\mu\text{-}PBu^t_2)_2]$ (5). Thermal treatment of 3 affords another complex of this latter type, $[Fe_2(CO)_5(\mu\text{-}PBu^t_2)(\mu\text{-}PPh_2)]$ (6). The structures of the three bis(phosphido)-bridged diiron complexes $[Fe_2(CO)_6(\mu\text{-}PBu^t_2)(\mu\text{-}PPh_2)]$ (3), $[Fe_2(CO)_5(\mu\text{-}PBu^t_2)(\mu\text{-}PPh_2)]$ (6), and $[Fe_2(CO)_5(\mu\text{-}PBu^t_2)_2]$ (5) have been determined by X-ray analysis. Crystal data for 3: monoclinic, space group $P2_1/c$, a = 10.143 (4) Å, b = 16.854 (8) Å, c = 16.871 (7) Å, β = 105.37 (3)°, Z = 4, R (R_w) = 0.035 (0.034). Crystal data for 6 at −95 °C: monoclinic, $P2_1/c$, a = 14.091 (7) Å, b = 12.090 (5) Å, c = 16.813 (7) Å, β = 112.60 (4)°, Z = 4, R (R_w) = 0.026 (0.033). Crystal data for 5: triclinic, $P\bar{1}$, a = 8.642 (5) Å, b = 11.730 (7) Å, c = 13.648 (9) Å, α = 76.61 (3)°, β = 78.76 (3)°, γ = 76.40 (4)°, Z = 2, R (R_w) = 0.033 (0.035). The electron-precise complex 3 has a strongly folded Fe_2P_2 core with a flap angle θ = 117.1° and an Fe–Fe distance of 2.707 (1) Å, whereas the two electron-deficient complexes 6 and 5 have only weakly folded or essentially planar Fe_2P_2 cores, respectively, and considerably shorter Fe–Fe distances (6, θ = 166.0°, Fe–Fe = 2.462 (1) Å; 5, θ = 176.2°, Fe–Fe = 2.484 (2) Å). EHMO calculations confirm that the short iron–iron bond distances in the bis(phosphido)-bridged diiron pentacarbonyl complexes are consistent with the presence of iron–iron double bonds.

Introduction

Recently we have confirmed ambident nucleophilicity for the phosphido-bridged diiron anions of the type $[Fe_2(\mu\text{-}CO)(CO)_6(\mu\text{-}PR_2)]^-$ by EHMO calculations, the nucleophilic centers being either the oxygen atom of the bridging carbonyl ligand or the iron–iron bond.[1] The reaction with $R_3O[BF_4]$[2] and $[M(PPh_3)Cl]$ (M = Cu, Ag, Au)[1,3] or H^+,[1] respectively, are examples of this ambidence.

Continuing this research, we report here on the metal-based nucleophilic reactions of these anions with R'_2PCl, which produce the well-known electron-precise type of complex $[Fe_2(CO)_6(\mu\text{-}PR_2)(\mu\text{-}PR'_2)]$[4] except for the case R = R' = Bu^t, where the bulkiness of these substituents gives rise to the new coordinatively unsaturated complex $[Fe_2(CO)_5(\mu\text{-}PBu^t_2)_2](Fe{=}Fe)$. This latter complex constitutes together with $[Co_2(CO)_4(\mu\text{-}PBu^t_2)_2]$[5] and $[Ni_2(CO)_3(\mu\text{-}PBu^t_2)_2]$,[6] described by Jones et al., a series of isoelectronic complexes.

In order to better understand the bonding of these unsaturated diiron complexes, an EHMO calculation has been carried out on the model complex $[Fe_2(CO)_5(\mu\text{-}PH_2)_2]$. X-ray structure analyses of $[Fe_2(CO)_5(\mu\text{-}PBu^t_2)_2]$ and also the electron-precise/-deficient pair of complexes $[Fe_2(CO)_n(\mu\text{-}PBu^t_2)(\mu\text{-}PPh_2)]$ (n = 6, 5) are presented.

Experimental Section

General Comments. All reactions were performed under oxygen-free argon using a conventional Schlenk technique. Solvents were dried over molecular sieves or over sodium/benzophenone ketyl and distilled under argon prior to use. Melting points were measured in sealed capillaries under argon and are uncorrected. Starting materials were either commercially available or were prepared according to literature procedures: Bu^t_2PCl,[7] Cy_2PCl,[8] Ph_2PCl,[9] Me_2PCl,[10] $Na[Fe_2(\mu\text{-}CO)(CO)_6(\mu\text{-}PR_2)]$.[1]

IR spectra were obtained using an IR 71 instrument by VEB Carl Zeiss Jena. ^1H and ^{31}P NMR spectra were recorded on the Bruker spectrometers WP 200 (^1H at 200.13 MHz, ^{31}P at 81.02

† Martin Luther University Halle-Wittenberg.
‡ University of Leipzig.
§ Technical University Braunschweig.
∥ Istituto per lo Studio dei Composti di Coordinazione.

(1) Walther, B.; Hartung, H.; Böttcher, H.-C.; Baumeister, U.; Böhland, U.; Sieler, J.; Reinhold, J.; Ladriere, J.; Schiebel, H.-M. *Polyhedron* **1991**, *10*, 2423.
(2) Osterloh, W. T. Ph.D. Thesis, University of Texas, Austin, TX, 1982; *Diss. Abstr. Int., B* **1982**.
(3) Ferrer, M.; Reina, R.; Rossell, O.; Seco, M.; Solans, X. *J. Chem. Soc., Dalton Trans.* **1991**, 347.
(4) See for instance: (a) Job, B. E.; McLean, R. A. N.; Thompson, D. T. *J. Chem. Soc., Chem. Commun.* **1966**, 895. (b) Collman, J. P.; Rothrock, R. K.; Finke, R. G.; Moore, E. J.; Rose-Munch, F. *Inorg. Chem.* **1982**, *21*, 146. (c) Teo, B.-K.; Hall, M. B.; Fenske, R. F.; Dahl, L. F. *Inorg. Chem.* **1975**, *14*, 3103. (d) Clegg, W. *Inorg. Chem.* **1976**, *15*, 1609. (e) Dessy, R. E.; Kornmann, R.; Smith, C.; Hayter, R. G. *J. Am. Chem. Soc.* **1968**, *90*, 2001. (f) Dessy, R. E.; Wieczorek, L. *J. Am. Chem. Soc.* **1969**, *91*, 4963. (g) Dessy, R. E.; Rheingold, A. L.; Howard, G. D. *J. Am. Chem. Soc.* **1972**, *94*, 746. (h) Dessy, R. E.; Bores, L. A. *Acc. Chem. Res.* **1972**, *5*, 415. (i) Burdett, J. K. *J. Chem. Soc., Dalton Trans.* **1977**, 423. (j) Ginsburg, R. E.; Rothrock, R. K.; Finke, R. G.; Collman, J. P.; Dahl, L. F. *J. Am. Chem. Soc.* **1979**, *101*, 6550. (k) Yu, Y.-F.; Gallucci, J.; Wojcicki, A. *J. Am. Chem. Soc.* **1983**, *105*, 4826. (l) Wojcicki, A. *Inorg. Chim. Acta* **1985**, *100*, 125. (m) Hayter, R. G. *Inorg. Chem.* **1964**, *3*, 711. (n) MacLaughlin, S. A.; Nucciarone, D.; Carty, A. J. In *Phosphorus-31 NMR Spectroscopy in Stereochemical Analysis: Organic Compounds and Metal Complexes*; Verkade, J. G., Quinn, L. D., Eds.; VCH: New York, 1986; Chapter 11, pp 559–619.
(5) Jones, R. A.; Stuart, A. L.; Atwood, J. L.; Hunter, W. E. *Organometallics* **1983**, *2*, 1437.
(6) Jones, R. A.; Stuart, A. L.; Atwood, J. L.; Hunter, W. E. *Organometallics* **1983**, *2*, 874.
(7) Field, M.; Stelzer, O.; Schmutzler, R. *Inorg. Synth.* **1973**, *14*, 4.
(8) Issleib, K.; Seidel, W. *Chem. Ber.* **1959**, *92*, 2681.
(9) Brown, M. P.; Silver, H. B. *Chem. Ind.* **1961**, 24.
(10) Parshall, G. W. *Inorg. Synth.* **1974**, *15*, 191.

0276-7333/92/2311-1542$03.00/0

Table I. Summary of Crystallographic Data for Compounds 3, 5, and 6

	3	6	5
empirical formula	$C_{26}H_{28}Fe_2O_6P_2$	$C_{25}H_{28}Fe_2O_5P_2$	$C_{21}H_{36}Fe_2O_5P_2$
mol wt	610.15	582.15	542.16
cryst syst	monoclinic	monoclinic	triclinic
space group	$P2_1/c$	$P2_1/c$	$P\bar{1}$
lattice constants			
a, Å	10.143 (4)	14.091 (7)	8.642 (5)
b, Å	16.854 (8)	12.090 (5)	11.730 (7)
c, Å	16.871 (7)	16.831 (7)	13.648 (9)
α, deg	90.0	90.0	76.31 (3)
β, deg	105.37 (3)	112.60 (4)	78.76 (3)
γ, deg	90.0	90.0	76.40 (4)
V, Å^3	2781 (2)	2644 (2)	1294 (2)
Z	4	4	2
$F(000)$	1256	1200	568
D_{calc}, g cm^{-3}	1.457	1.462	1.392
μ(Mo Kα), cm^{-1}	11.9	12.5	12.7
cryst dimens, mm	0.39 × 0.30 × 0.09	1.00 × 0.60 × 0.35	0.29 × 0.24 × 0.23
diffractometer	Huber	Siemens	Huber
temp, K	293	178	293
check rflns	$2\bar{4}2$, 020	108, 064, $\bar{6}40$	$0\bar{2}6$, $0\bar{1}5$
intens variation, %	±3.2, ±2.3	±1.6	±3.3, ±2.8
no. of unique rflns	4906	4651	4565
range of measurement, deg	$2 \le 2\theta \le 52$	$6 \le 2\theta \le 50$	$2 \le 2\theta \le 50$
min hkl	$0,0,\overline{20}$	$\overline{16},\overline{14},0$	$\bar{9},\overline{13},0$
max hkl	12,20,20	15,3,19	10,13,16
no. of rflns obsd	2854 ($I \ge 1.96\sigma(I)$)	4100 ($I \ge 2.00\sigma(I)$)	3565 ($I \ge 1.96\sigma(I)$)
no. of rflns/param	7.7	12.6	8.6
weighting scheme	$w = 1/\sigma^2(F_o)$	$w = 1/\sigma^2(F_o) + 0.0002F_o^2$	$w = 1/\sigma^2(F_o)$
max shift/σ (last least-squares cycle)	2.33	0.009	0.24
max/min $\Delta\rho$ in diff map, e Å^{-3}	+0.37/−0.29	+0.34/−0.33	+0.49/−0.41
R (R_w)	0.035 (0.034)	0.026 (0.033)	0.033 (0.035)
goodness of fit (S)	1.64	1.58	2.11

MHz) and AC 80 (^{1}H at 80.13 MHz, ^{31}P at 32.43 MHz). Chemical shift references are the absolute frequencies of Me_4Si (^{1}H) and external 85% H_3PO_4(aq) (^{31}P), respectively. Positive shifts are to lower field. The mass spectra were obtained with a Hewlett-Packard 5995A spectrometer. The electronic spectra were run in pentane solution ($c = 2 \times 10^{-4}$ mol L^{-1}) on the UV/vis M40 spectrometer by VEB Carl Zeiss Jena.

Synthesis of $[Fe_2(CO)_n(\mu\text{-}PR_2)(\mu\text{-}PR'_2)]$ (n = 6, 1–4; n = 5, 5). A solution of 1 mmol of the sodium salt $Na[Fe_2(\mu\text{-}CO)(CO)_6(\mu\text{-}PR_2)]$ (0.52 g (R = Ph), 0.53 g (Cy), 0.39 g (Me), 0.48 g (Bu^t)) and 1 mmol of R'_2PCl (0.22 g of Ph_2PCl, 0.18 g of Bu^t_2PCl, 0.24 g of Cy_2PCl) in 30 mL of THF was refluxed for 4 h. After it was cooled to 25 °C, the orange-yellow (1, 2), deep red-brown (3, 4), and deep green (5) solution, respectively, was filtered and evaporated to dryness. The residue was extracted three times with 20 mL of pentane. The extracts were combined, and the volume was reduced in vacuo to 10 mL. In the case of 3 the residue from THF was washed with 10 mL of pentane and extracted with Et_2O. 1–5 crystallized at −78 °C.

1: 0.55 g, 83%; mp 190–195 °C dec. Anal. Calcd for $C_{30}H_{32}Fe_2O_6P_2$: C, 54.38; H, 4.83; P, 9.37. Found: C, 53.95; H, 5.10; P, 9.39. MS: m/e 662 (M$^+$). ^{1}H NMR (acetone-d_6): δ 1.2–2.3 (m, Cy), 7.53 (m, Ph). UV/vis: λ_{max} = 405 nm (ϵ_0 = 1900), 285 (7500).

2: 0.5 g, 74%; mp 265–267 °C dec. Anal. Calcd for $C_{30}H_{44}Fe_2O_6P_2$: C, 53.44; H, 6.53; P, 9.19. Found: C, 53.30; H, 6.43; P, 8.90. MS: m/e 674 (M$^+$). UV/vis: λ_{max} = 420 nm (ϵ_o = 1920), 285 (6760), 235 (11 200).

3: 0.3 g, 50%; mp 165–170 °C dec. Anal. Calcd for $C_{26}H_{28}Fe_2O_6P_2$: C, 51.15; H, 4.59; P, 10.16. Found: C, 51.93; H, 4.72; P, 10.24. MS: m/e 610 (M$^+$). ^{1}H NMR (acetone-d_6): δ 1.38 (d, ^3J(PH) = 14.3 Hz), 7.53 (m, Ph). UV/vis: λ_{max} = 485 nm (ϵ_o = 2200), 305 (sh).

4: 0.3 g, 61%; mp 175–180 °C dec. Anal. Calcd for $C_{16}H_{24}Fe_2O_6P_2$: C, 39.51; H, 4.94; P, 12.76. Found: C, 38.78; H, 5.35; P, 12.76. MS: m/e 486 (M$^+$). ^{1}H NMR (C_6D_6): δ 1.51 (d, ^2J(PH) = 11.0 Hz, Me), 1.24 (d, ^3J(PH) = 13.9 Hz, Bu^t).

5: 0.34 g, 63%; mp 196–198 °C dec (from diethyl ether). Anal. Calcd for $C_{21}H_{36}Fe_2O_5P_2$: C, 46.52; H, 6.64; P, 11.43. Found: C, 45.99; H, 6.75; P, 10.90. MS: m/e 542 (M$^+$). ^{1}H NMR (C_6D_6): δ 1.25 (d, ^3J(PH) = 9.3 Hz). UV/vis: λ_{max} = 659 nm (ϵ_o = 1500), 465 (700), 327 (5600).

Synthesis of $[Fe_2(CO)_5(\mu\text{-}PBu^t_2)(PPh_2)]$ (6). A solution of highly purified 3 (305 mg, 0.5 mmol) in toluene was boiled for 5 h, while argon was bubbled through the solution. During this time the color of the mixture changes from brown to deep green. Subsequently the solution was cooled to room temperature, filtered, and evaporated to dryness. The residue was extracted twice with 15 mL of pentane, and the combined extracts were reduced in volume to 5 mL. Black-green crystals of 6 were obtained at −78 °C: yield up to 290 mg, 100%; mp 135–140 °C dec. Anal. Calcd for $C_{25}H_{28}Fe_2O_5P_2$: P, 10.65. Found: P, 10.62. ^{1}H NMR ($CDCl_3$): δ 1.32 (d, ^3J(PH) = 14.6 Hz, Bu^t), 7.42 (m, Ph). UV/vis: λ_{max} = 664 (ϵ_o = 1200), 455 (1400), 349 (9200). 6 is extremely sensitive to air and traces of grease. Solutions in pentane are less stable than those in diethyl ether and THF.

X-ray Crystallography. A summary of crystal data along with details of the structure determinations is given in Table I. All measurements were performed using graphite-monochromated Mo Kα radiation. The data sets for 3 and 5 were measured on a Huber four-circle diffractometer in the $\theta/2\theta$ scanning mode at room temperature; that of 6 was measured on a Siemens R3m/V diffractometer in the ω-scan mode with cooling by a nitrogen stream. Lattice constants were obtained by a least-squares treatment of the setting angles of 16, 13, and 50 reflections for 3, 5, and 6, respectively. Lorentz and polarization corrections were applied during data reduction; absorption effects were neglected in the cases of 3 and 5. For compound 6 an empirical absorption correction based on ψ-scan measurements was performed with maximum and minimum transmission factors of 0.848 and 0.640, respectively. The structures of 3 and 6 were solved by Patterson methods (program systems SHELXS-86[11] and Siemens SHELXTL PLUS[12]); that of 5 was solved by direct methods (SHELXS-86[11]). Structure refinement on F was performed using the full-matrix least-squares techniques of SHELX-76[13] (in the cases of 3 and 5) and SHELXTL PLUS[12] (in the case of 6). All non-H positions were

(11) Sheldrick, G. M. SHELXS-86, Program for crystal structure determination; University of Göttingen: Göttingen, FRG, 1986.
(12) Sheldrick, G. M. SHELXTL PLUS, Software package for solution and refinement of small-molecule single crystals, Version 4.2; Siemens Analytical X-ray Instruments: Madison, WI, 1990.
(13) Sheldrick, G. M. SHELX-76, Program for crystal structure determination; University of Cambridge: Cambridge, England, 1976.

Table II. Fractional Coordinates and Equivalent Isotropic Displacement Parameters (Å²) for the Non-Hydrogen Atoms of 3

atom	x/a	y/b	z/c	U_{eq}[a]
Fe1	0.16651 (6)	0.30074 (3)	0.11591 (3)	0.0318 (2)
Fe2	0.28669 (6)	0.36372 (3)	0.00493 (3)	0.0330 (2)
P1	0.39165 (11)	0.30057 (7)	0.12245 (6)	0.0330 (4)
P2	0.11140 (11)	0.27345 (6)	−0.01921 (6)	0.0313 (3)
O1	0.1854 (4)	0.4534 (2)	0.2032 (2)	0.058 (1)
O2	0.1973 (4)	0.1556 (2)	0.2135 (3)	0.075 (2)
O3	−0.1179 (4)	0.3039 (3)	0.1223 (2)	0.073 (2)
O4	0.1470 (5)	0.4849 (2)	−0.1119 (3)	0.081 (2)
O5	0.4239 (4)	0.5111 (2)	0.0764 (2)	0.070 (2)
O6	0.4449 (4)	0.3084 (2)	−0.1062 (2)	0.069 (2)
C1	0.1852 (4)	0.3940 (3)	0.1706 (3)	0.039 (2)
C2	0.1874 (5)	0.2126 (3)	0.1754 (3)	0.045 (2)
C3	−0.0087 (5)	0.3044 (3)	0.1147 (3)	0.045 (2)
C4	0.1895 (5)	0.4348 (3)	−0.0675 (3)	0.052 (2)
C5	0.3740 (5)	0.4525 (3)	0.0514 (3)	0.043 (2)
C6	0.3847 (5)	0.3287 (3)	−0.0613 (3)	0.045 (2)
C7	0.5033 (4)	0.3585 (3)	0.2074 (3)	0.038 (2)
C8	0.6208 (5)	0.3959 (3)	0.1968 (3)	0.052 (2)
C9	0.7037 (5)	0.4390 (3)	0.2604 (4)	0.063 (2)
C10	0.6706 (6)	0.4453 (3)	0.3344 (4)	0.061 (2)
C11	0.5603 (6)	0.4070 (3)	0.3469 (3)	0.060 (2)
C12	0.4747 (5)	0.3634 (3)	0.2836 (3)	0.045 (2)
C13	0.5047 (4)	0.2137 (2)	0.1321 (3)	0.035 (1)
C14	0.5143 (5)	0.1599 (3)	0.1960 (3)	0.044 (2)
C15	0.6003 (5)	0.0952 (3)	0.2047 (3)	0.051 (2)
C16	0.6790 (5)	0.0829 (3)	0.1504 (3)	0.056 (2)
C17	0.6736 (5)	0.1368 (3)	0.0882 (3)	0.056 (2)
C18	0.5867 (5)	0.2020 (3)	0.0787 (3)	0.048 (2)
C19	−0.0597 (5)	0.3133 (3)	−0.0875 (3)	0.045 (2)
C20	−0.1802 (5)	0.2564 (4)	−0.0927 (4)	0.062 (2)
C21	−0.0472 (6)	0.3283 (4)	−0.1762 (3)	0.061 (2)
C22	−0.0972 (5)	0.3923 (3)	−0.0514 (3)	0.054 (2)
C23	0.1264 (5)	0.1657 (3)	−0.0513 (3)	0.041 (2)
C24	0.2738 (5)	0.1378 (3)	−0.0159 (3)	0.052 (2)
C25	0.0346 (6)	0.1115 (3)	−0.0153 (4)	0.059 (2)
C26	0.0918 (6)	0.1546 (3)	−0.1457 (3)	0.058 (2)

[a] $U_{eq} = {}^1/_3\sum_i\sum_j U_{ij}a^*_i a^*_j \mathbf{a}_i\cdot\mathbf{a}_j$.

refined with anisotropic displacement parameters; those of the H atoms of **5** were refined with isotropic parameters in a separate block. The H atom positions for **3** and **6** were determined by geometric calculations, with methyl groups treated as rigid groups and the others as riding atoms in the sense of the SHELX program. The observed structure factors of **5** were corrected by the empirical extinction coefficient χ with χ refined to 1.56 (6) × 10^{-7}. Final non-H atomic parameters are summarized in Tables II–IV.

Results and Discussion

Synthesis. The reactions of $Na[Fe_2(\mu\text{-}CO)(CO)_6(\mu\text{-}PR_2)]$ with R'_2PCl in THF proceed according to eq 1 and give bis(phosphido)-bridged diiron complexes containing usually six, but in the case R = R′ = Bu^t only five, carbonyl ligands. Compounds **1**–**4** belong to the well-established

$$[Fe_2(\mu\text{-}CO)(CO)_6(\mu\text{-}PR_2)]^- + R'_2PCl \xrightarrow[-Cl^-]{} \underset{\mathbf{1-5}}{[Fe_2(CO)_n(\mu\text{-}PR_2)(\mu\text{-}PR'_2)]} \quad (1)$$

	1	2	3	4	5
n	6	6	6	6	5
R	Ph	Cy	Ph	Me	Bu^t
R′	Cy	Cy	Bu^t	Bu^t	Bu^t

family of bis(phosphido)-bridged diiron hexacarbonyl complexes,[4] of which the first example (R = R′ = Ph) was prepared by Thompson et al. in 1966.[4a] The metal-centered reactions (1) allow easy preparation of such complexes with different phosphido bridges.

Obviously, the bulk of the *tert*-butyl substituents on both phosphorus atoms causes the formation of the coordinatively unsaturated complex **5**. This complex does not coordinate a further CO ligand even under 80 atm of carbon monoxide. Whereas **2** does not lose one carbonyl ligand to give $[Fe_2(CO)_5(\mu\text{-}PCy_2)_2]$ either by thermal or photolytic means or via reaction with Me_3NO, complex **3** does exist in a thermal equilibrium with the related unsaturated complex **6** as shown in eq 2. An analogous

$$3 \underset{\text{room temp, +CO}}{\overset{\Delta\text{ (toluene), −CO}}{\rightleftharpoons}} \underset{\mathbf{6}}{[Fe_2(CO)_5(\mu\text{-}PPh_2)(\mu\text{-}PBu^t_2)]} \quad (2)$$

equilibrium could not be detected with complex **4**. The new compounds were characterized by elemental analysis and by UV/vis, IR, and NMR spectroscopy and mass spectrometry. Single-crystal X-ray diffraction studies of complexes **3**, **5**, and **6** were carried out mainly in order to elucidate the structural features caused by the loss of one two-electron ligand on going from **3** to **6**.

Spectroscopy. In contrast to the bright yellow complexes **1** and **2**, **3** and **4** are deep red-brown, and **5** and **6** are black-green in the solid state and dark green in solution. The pentane solutions of these complexes accordingly show characteristic absorptions in the visible spectra with λ_{max} at 420 nm (ϵ_0 = 1920) (**1**), 405 (1900) (**2**), 485 (2200) (**3**), 460 (3900) (**4**), and 659 (1500) (**6**), respectively. Thus, the electronically saturated complexes **1**–**4** exhibit bands at lower wavelength than the unsaturated complex **5**, where this band is assigned to the $\pi \rightarrow \pi^*$ transition according to the EHMO calculation (see below).

The IR and $^{31}P\{^1H\}$ NMR data are summarized in Table V. The IR spectra show five bands in the region typical of terminal ligands. The ^{31}P NMR spectra consist either of a singlet (R = R′) or of a double doublet of the AX type (R ≠ R′). The pronounced downfield shift of these resonances indicates phosphido groups bridging a metal–metal bond.[14–16] The proton-coupled spectra allow the

Table III. Fractional Coordinates and Equivalent Isotropic Displacement Parameters (Å²) for the Non-Hydrogen Atoms of 6

atom	x/a	y/b	z/c	U_{eq}[a]
Fe1	0.70939 (2)	0.25525 (2)	0.59133 (2)	0.0223 (1)
Fe2	0.73053 (2)	0.17725 (2)	0.46385 (2)	0.0217 (1)
P1	0.66178 (4)	0.34836 (4)	0.47545 (3)	0.0230 (2)
P2	0.79590 (4)	0.10586 (4)	0.60568 (3)	0.0225 (2)
O1	0.5307 (1)	0.2248 (2)	0.6346 (1)	0.0667 (9)
O2	0.8132 (2)	0.3948 (1)	0.7398 (1)	0.0662 (8)
O4	0.8003 (1)	−0.0420 (1)	0.4356 (1)	0.0376 (6)
O5	0.5318 (1)	0.1168 (1)	0.3282 (1)	0.0584 (7)
O6	0.8519 (2)	0.2881 (2)	0.3792 (1)	0.0724 (11)
C1	0.6024 (2)	0.2374 (2)	0.6184 (1)	0.0381 (9)
C2	0.7716 (2)	0.3402 (2)	0.6806 (1)	0.0377 (8)
C4	0.7770 (2)	0.0437 (2)	0.4520 (1)	0.0279 (7)
C5	0.6083 (2)	0.1435 (2)	0.3807 (1)	0.0357 (8)
C6	0.8042 (2)	0.2446 (2)	0.4113 (2)	0.0393 (9)
C7	0.5305 (2)	0.3706 (2)	0.3999 (1)	0.0249 (7)
C8	0.5072 (2)	0.3767 (2)	0.3111 (1)	0.0308 (7)
C9	0.4062 (2)	0.3882 (2)	0.2537 (1)	0.0341 (8)
C10	0.3281 (2)	0.3948 (2)	0.2837 (1)	0.0368 (8)
C11	0.3501 (2)	0.3911 (2)	0.3712 (1)	0.0358 (8)
C12	0.4508 (2)	0.3780 (2)	0.4293 (1)	0.0283 (7)
C13	0.7283 (2)	0.4735 (2)	0.4642 (1)	0.0258 (7)
C14	0.6774 (2)	0.5645 (2)	0.4155 (1)	0.0337 (8)
C15	0.7381 (2)	0.6605 (2)	0.4146 (2)	0.0421 (10)
C16	0.8364 (2)	0.6666 (2)	0.4611 (2)	0.0412 (10)
C17	0.8878 (2)	0.5771 (2)	0.5100 (2)	0.0403 (9)
C18	0.8346 (2)	0.4816 (2)	0.5117 (1)	0.0336 (8)
C19	0.7433 (2)	−0.0303 (2)	0.6274 (1)	0.0322 (8)
C20	0.7322 (2)	−0.0191 (2)	0.7148 (1)	0.0428 (9)
C21	0.8080 (2)	−0.1329 (2)	0.6293 (2)	0.0461 (10)
C22	0.6355 (2)	−0.0467 (2)	0.5579 (2)	0.0418 (9)
C23	0.9416 (2)	0.1072 (2)	0.6589 (1)	0.0310 (7)
C24	0.9776 (2)	0.2255 (2)	0.6521 (2)	0.0445 (9)
C25	0.9777 (2)	0.0782 (2)	0.7551 (1)	0.0427 (9)
C26	0.9934 (2)	0.0312 (2)	0.6143 (1)	0.0418 (9)

[a] See footnote *a* in Table II.

Table IV. Fractional Coordinates and Equivalent Isotropic Displacement Parameters (Å²) for the Non-Hydrogen Atoms of 5

atom	x/a	y/b	z/c	U_{eq}[a]
Fe1	0.14297 (4)	0.26657 (3)	0.32952 (3)	0.032 (3)
Fe2	0.31560 (4)	0.31951 (3)	0.16433 (3)	0.033 (3)
P1	0.26155 (8)	0.12936 (6)	0.24574 (6)	0.036 (4)
P2	0.16035 (8)	0.44943 (6)	0.27291 (5)	0.031 (4)
O1	0.1843 (3)	0.1891 (2)	0.5426 (2)	0.068 (9)
O2	−0.1936 (3)	0.2515 (3)	0.3897 (2)	0.072 (9)
O4	0.3032 (3)	0.5450 (2)	0.0188 (2)	0.071 (9)
O5	0.6506 (3)	0.3054 (3)	0.1855 (2)	0.074 (9)
O6	0.4068 (4)	0.2125 (3)	−0.0167 (2)	0.087 (10)
C1	0.1714 (4)	0.2197 (3)	0.4578 (2)	0.043 (9)
C2	−0.0608 (4)	0.2575 (3)	0.3636 (2)	0.046 (9)
C4	0.3007 (4)	0.4598 (3)	0.0797 (2)	0.046 (9)
C5	0.5201 (4)	0.3092 (3)	0.1809 (2)	0.045 (9)
C6	0.3653 (4)	0.2486 (3)	0.0573 (3)	0.055 (10)
C7	0.4446 (4)	0.0143 (3)	0.2851 (3)	0.050 (9)
C8	0.5730 (4)	−0.0101 (4)	0.1938 (3)	0.069 (11)
C9	0.5189 (4)	0.0624 (3)	0.3563 (3)	0.056 (10)
C10	0.3967 (5)	−0.1023 (3)	0.3456 (4)	0.080 (12)
C13	0.1366 (4)	0.0592 (3)	0.1843 (3)	0.051 (9)
C14	0.2319 (5)	−0.0236 (4)	0.1119 (3)	0.069 (11)
C15	0.0328 (5)	−0.0109 (4)	0.2700 (4)	0.071 (11)
C16	0.0240 (4)	0.1616 (4)	0.1250 (3)	0.068 (11)
C19	0.2859 (4)	0.5278 (3)	0.3257 (2)	0.042 (9)
C20	0.1805 (4)	0.6105 (3)	0.3946 (3)	0.057 (10)
C21	0.3899 (4)	0.5995 (3)	0.2403 (3)	0.055 (10)
C22	0.3979 (4)	0.4315 (3)	0.3910 (3)	0.055 (10)
C23	−0.0208 (3)	0.5625 (3)	0.2254 (2)	0.041 (9)
C24	−0.0873 (4)	0.5084 (3)	0.1548 (3)	0.053 (10)
C25	−0.1511 (4)	0.5769 (3)	0.3183 (3)	0.053 (9)
C26	0.0104 (4)	0.6857 (3)	0.1696 (3)	0.058 (10)

[a] See footnote *a* in Table II.

Table V. IR and $^{31}P\{^1H\}$ NMR Data for Complexes 1–6

complex	ν(CO), cm⁻¹[a]	δ, ppm	^2J(PP), Hz
1	2050 vs, 2012 vs, 1984 vs, 1964 vs, 1954 w	170.4[b] 150.7	115.1
2	2040 vs, 2002 vs, 1968 vs, 1962 vs, 1956 m	180.4[c]	
3	2044 s, 2004 vs, 1964 w, 1956 s, 1946 w	294.4[b] 173.7	64.0
4	2038 s, 2000 vs, 1968 s, 1960 s, 1944 s	353.8[b] 162.8	37.5
5	2014 s, 1960 vs, 1954 vs, 1910 vs	364.0[b]	60.3
6	2026 s, 2004 m, 1966 vs, 1954 s, 1922 s	354.8[b] 256.8	

[a] Hexane. [b] THF. [c] Benzene.

assignment of the signal at lower field to the μ-PCy_2 (1) and μ-PBu^t_2 groups (3, 4, 6), respectively. Noteworthy is the further downfield shift of the signal of the μ-PBu^t_2 group as one goes from the electron-precise complex 3 to the electron-deficient complex 6. This can be correlated with the more acute bond angles Fe1–P–Fe2 and the shorter Fe–Fe bond length in 6.

The mass spectra of 1–5 exhibit molecular peaks, but for 3 and 4 these peaks are of very low intensity (<1%) whereas the $(M - CO)^+$ peak appears with the expected high intensity.

Molecular Structures. The molecular structures of 3, 6, and 5 are shown in Figures 1–3, respectively, with selected bond lengths and angles in Table VI.

Structure of 3. The basic geometry of the electron-precise complex 3 (Figure 1) agrees qualitatively with that observed in other bis(μ-phosphido)hexacarbonyldiiron complexes:[4] the molecular core consists of two iron atoms linked by two bridging P atoms and is highly nonplanar, being folded about the Fe–Fe bond or about the P···P line ("butterfly" geometry). In 3 the coordination spheres of both iron atoms are (neglecting Fe–Fe bonding) distorted-tetragonal pyramids joined along the P1···P2 basal edge with C2 and C6 located in the apical positions. The steric

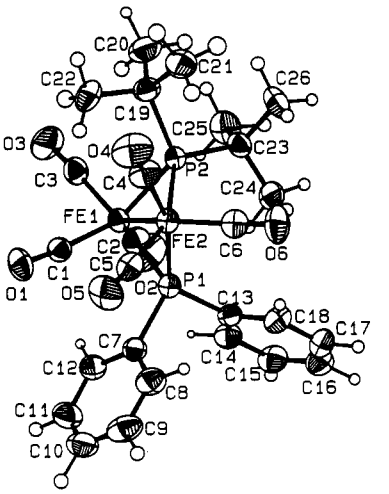

Figure 1. Molecular structure of $[Fe_2(CO)_6(\mu\text{-}PBu^t_2)(\mu\text{-}PPh_2)]$ (3) with atom labels.

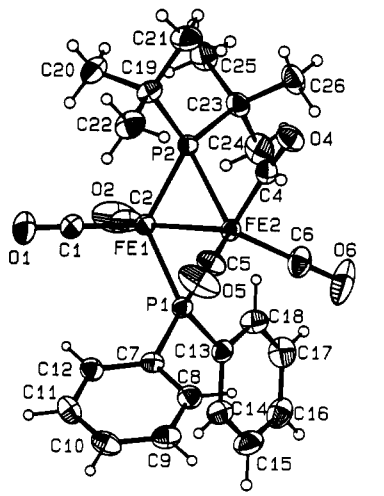

Figure 2. Molecular structure of $[Fe_2(CO)_5(\mu\text{-}PBu^t_2)(\mu\text{-}PPh_2)]$ (6) with atom labels.

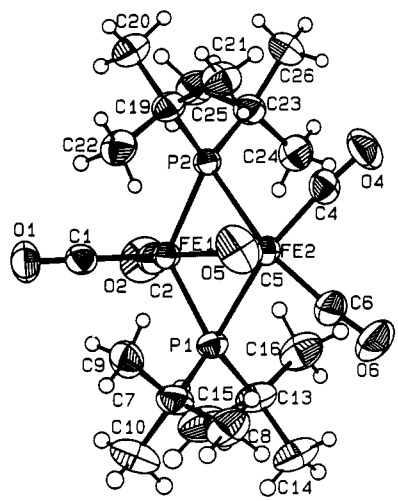

Figure 3. Molecular structure of $[Fe_2(CO)_5(\mu\text{-}PBu^t_2)_2]$ (5) with atom labels.

(14) Garrou, P. E. *Chem. Rev.* **1981**, *81*, 229.
(15) Carty, A. J. *Adv. Chem. Ser.* **1982**, *No. 196*, 163.
(16) Geoffroy, G. L. *Organometallics* **1983**, *2*, 53.

Table VI. Selected Bond Lengths (Å) and Angles (deg) for Compounds 3, 5, and 6

	3	6	5
Fe1-Fe2	2.707 (1)	2.462 (1)	2.484 (2)
Fe1-P1	2.257 (2)	2.123 (1)	2.135 (2)
Fe1-P2	2.246 (2)	2.140 (1)	2.135 (2)
Fe2-P1	2.252 (2)	2.324 (1)	2.360 (2)
Fe2-P2	2.293 (2)	2.365 (1)	2.372 (2)
Fe1-C1	1.808 (5)	1.747 (2)	1.757 (3)
Fe1-C2	1.774 (5)	1.750 (2)	1.753 (3)
Fe1-C3	1.773 (5)		
Fe2-C4	1.806 (5)	1.782 (2)	1.771 (3)
Fe2-C5	1.808 (5)	1.799 (2)	1.798 (3)
Fe2-C6	1.782 (6)	1.796 (3)	1.777 (4)
P1-Fe1-P2	91.48 (8)	121.08 (2)	122.06 (3)
P1-Fe2-P2	90.35 (7)	104.70 (2)	104.36 (3)
Fe1-P1-Fe2	73.77 (7)	67.06 (2)	66.85 (3)
Fe1-P2-Fe2	73.21 (6)	66.05 (2)	66.64 (3)
P1-Fe1-C1	90.5 (2)	107.72 (8)	110.3 (1)
P1-Fe1-C2	90.2 (2)	110.68 (8)	108.4 (1)
P1-Fe1-C3	177.2 (2)		
P2-Fe1-C1	131.4 (2)	112.16 (8)	112.1 (1)
P2-Fe1-C2	111.3 (2)	108.81 (7)	108.9 (1)
P2-Fe1-C3	91.0 (2)		
C1-Fe1-C2	117.3 (2)	92.74 (11)	90.4 (2)
C1-Fe1-C3	86.8 (2)		
C2-Fe1-C3	90.3 (2)		
P1-Fe2-C4	162.6 (2)	177.18 (7)	159.3 (1)
P1-Fe2-C5	86.9 (2)	87.81 (7)	103.7 (1)
P1-Fe2-C6	100.6 (2)	88.62 (7)	80.9 (1)
P2-Fe2-C4	93.5 (2)	76.38 (7)	78.7 (1)
P2-Fe2-C5	153.3 (2)	125.94 (8)	104.4 (1)
P2-Fe2-C6	101.8 (2)	125.91 (8)	157.2 (1)
C4-Fe2-C5	82.0 (2)	89.46 (9)	95.2 (2)
C4-Fe2-C6	95.2 (2)	92.83 (10)	88.9 (2)
C5-Fe2-C6	104.8 (5)	106.38 (11)	95.7 (2)
Fe1-C1-O1	174.3 (5)	178.7 (2)	177.6 (2)
Fe1-C2-O2	178.2 (5)	179.1 (2)	177.4 (3)
Fe1-C3-O3	172.8 (4)		
Fe2-C4-O4	169.6 (5)	173.0 (2)	173.3 (2)
Fe2-C5-O5	175.5 (4)	176.7 (2)	176.0 (3)
Fe2-C6-O6	177.1 (4)	179.0 (2)	172.5 (3)

effects due to the bulky *tert*-butyl substituents at P2 cause significant deviations of the values for the geometrical parameters of **3** compared with those of the well-known $[Fe_2(CO)_6(\mu\text{-}PRR')_2]$ complexes compiled by Clegg.[4d] The fold of the Fe_2P_2 ring is commonly expressed by the dihedral angle θ between the two FeP_2 planes.[4j] Its value of 117.1° in **3** is considerably larger than the values observed for complexes with R, R′ = C_6H_5, CH_3, H (θ = 100.0–107.3°)[4d] but is comparable with θ = 118.9° in the case of the electron-withdrawing substituent R = R′ = CF_3. Moreover, the Fe–Fe distance of 2.707 (1) Å in **3** lies above the range observed for the aforementioned series (2.619–2.665 Å)[4d] but is smaller than in the trifluoromethyl compound (2.819 (1) Å).[4d] The Fe–P–Fe angles in **3** are highly acute and are in good agreement with the majority of other related complexes, whereas the P···P distance (3.225 (2) Å) and mean Fe–P bond lengths and P–Fe–P angles (2.262 Å and 90.9°, respectively) are significantly enlarged. The steric crowding of the PBu^t_2 ligand is clearly evident from the 13° shrinkage of the angle C7–P1–C13 (96.4 (2)°) from a normal tetrahedral angle and the significant deviation from linearity of the nonapically oriented Fe–C–O chains (cf. Table VI). Geometric bond parameters of the phenyl and *tert*-butyl groups are as expected.

Structure of 6. The complex **6**, with a total of only five CO groups, is the electron-deficient counterpart of the electron-precise complex **3** and thus was expected to show exact planarity of the Fe_2P_2 core, according to the structures observed for the isoelectronic compounds $[Co_2(CO)_4(\mu\text{-}PBu^t_2)_2]$[5] and $[Ni_2(CO)_3(\mu\text{-}PBu^t_2)_2]$.[6] However, a remarkable nonplanarity with a flap angle θ = 166.0° with respect to the P···P line was found. The Fe–Fe bond length of 2.462 (1) Å is very short (no shorter Fe–Fe distance for a bis(phosphido)-bridged diiron complex has been reported) and indicates a strong interaction (see below). The atom Fe1, bearing only two terminal CO ligands, has (ignoring the Fe–Fe bond) an approximately tetrahedral coordination sphere. Its electron deficiency is counterbalanced mainly by the short Fe1–P bond lengths (Fe1–P(av) = 2.132 Å compared with Fe2–P(av) = 2.344 Å), but the Fe–C bonds could also contribute to some extent (Fe1–C(av) = 1.748 Å, Fe2–P(av) = 1.792 Å). The Fe2 atom obeys the 18-electron rule, and its coordination sphere may be described as a strongly distorted tetragonal pyramid (as in **3**) with C5 at the apical position. The coordination polyhedra are fused along P1···P2. The short Fe–Fe bond distance gives rise to very acute Fe–P–Fe angles (average 66.56°), agreeing well with the corresponding values for the above-mentioned isoelectronic Co complex (Co–P–C = 66.83 (9)°)[5] and Ni complex (Ni–P–Ni = 66.83 (9)°),[6] and to rather large P–Fe–P angles (cf. Table VI). Of the five CO ligands in **6**, only the Fe2C4O4 group deviates appreciably from linearity. This may be interpreted as a sign of lower steric strain in **6**, attributable to both the loss of one CO group and the flattening of the Fe_2P_2 core compared with that of **3**.

Structure of 5. Compound **5** is related to **6** by substitution of the two phenyl groups at P1 by two *tert*-butyl groups, resulting in an electron-deficient complex with two identical bulky bridging phosphido ligands. Its molecular structure is very similar to that of **6**; the corresponding bond lengths and angles are in very good agreement (cf. Table VI; average values Fe1–P = 2.136 Å, Fe2–P = 2.366 Å, Fe1–C = 1.755 Å, Fe2–C = 1.782 Å, Fe–P–Fe = 66.75°). Some striking differences discussed in the following arise mainly from the higher molecular symmetry and the bulkiness of the four *tert*-butyl groups. The Fe_2P_2 core is essentially planar (sum of the endocyclic angles at the Fe and P atoms 359.9°) and only very slightly folded along P1···P2 (θ = 176.2°). The molecule has C_s symmetry to a good approximation, with a noncrystallographic mirror plane containing both Fe atoms, the two CO ligands at Fe1 and the C5O5 ligand at Fe2. Thus, Fe2 has also a distorted-tetragonal-pyramidal coordination sphere with C5 in an apical position, but the individual P–Fe2–C angles are quite different from those in **6**. Because of the symmetrical arrangement and bulkiness of the four *tert*-butyl groups not only the C4O4 but also the C6O6 carbonyl ligand attached to Fe2 are subject to steric strain (cf. Fe–C–O angles in Table V).

There are no indications of special intermolecular interactions beyond van der Waals distances within the crystal structures of the three compounds.

EHMO Calculations. Formal electron counting predicts a net iron–iron bond order of 2 for complexes of the type $[Fe_2(CO)_5(\mu\text{-}PR_2)_2]$, which can be directly related to the short Fe–Fe bond distances of complexes **5** and **6**. In addition to the Fe–Fe σ-bond there should be a second bond, probably of π type. This can be formally considered as due to an electron pair donated from the electron-rich (18e) iron atom (Fe2) to the 16e iron atom (Fe1). We have carried out extended Hückel molecular orbital calculations[17] with fragment molecular orbital analysis to obtain

(17) (a) Hoffmann, R.; Lipscomb, W. N. *J. Chem. Phys.* **1962**, *36*, 2179, 3489. (b) Hoffmann, R. *J. Chem. Phys.* **1963**, *39*, 1397. Standard atomic parameters were used for the calculations. The geometries for the models match those of the X-ray diffraction study reported in the present paper.

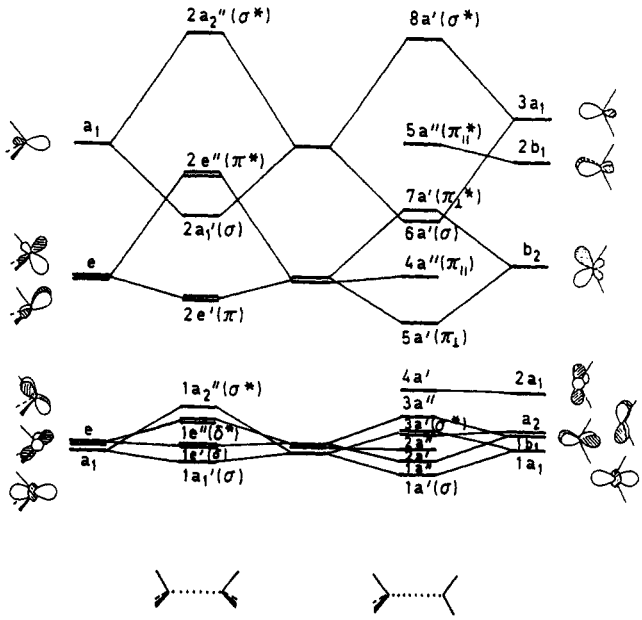

Figure 4. Interaction diagram between $Fe(CO)_3$ and $Fe(CO)_2$ fragments as compared with the case of two interacting $Fe(CO)_3$ fragments.

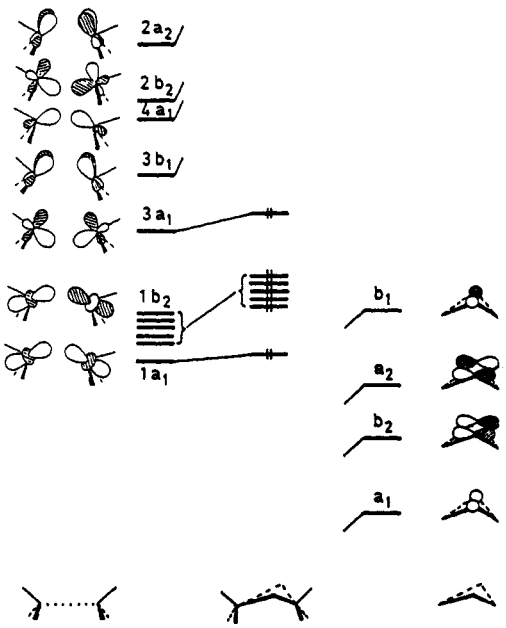

Figure 5. Interaction diagram between a $Fe_2(CO)_6$ fragment and two bridging non-coplanar PH_2 ligands.

a more detailed insight into the bonding properties of these complexes. The strategy used to study how the Fe–P_{bridge} bonds and the direct Fe–Fe bonds arise is to analyze the interactions between the fragment formed by the metals and terminal ligands with that formed by the bridges alone.

Figure 4 shows how the fragment molecular orbitals of $Fe_2(CO)_5$ are built up from the frontier orbitals of typical ML_3 and ML_2 fragments (see, e.g., ref 18). As a comparison, we also present the well-known fragment molecular orbitals of $Fe_2(CO)_6$ (see, e.g., ref 19), which are merely the in-phase and out-of-phase combinations of the orbitals of two ML_3 fragments.

Indeed, complexes of the type $[Fe_2(CO)_6(\mu\text{-}PR_2)_2]$ are found to contain a nonplanar Fe_2P_2 core. A theoretical

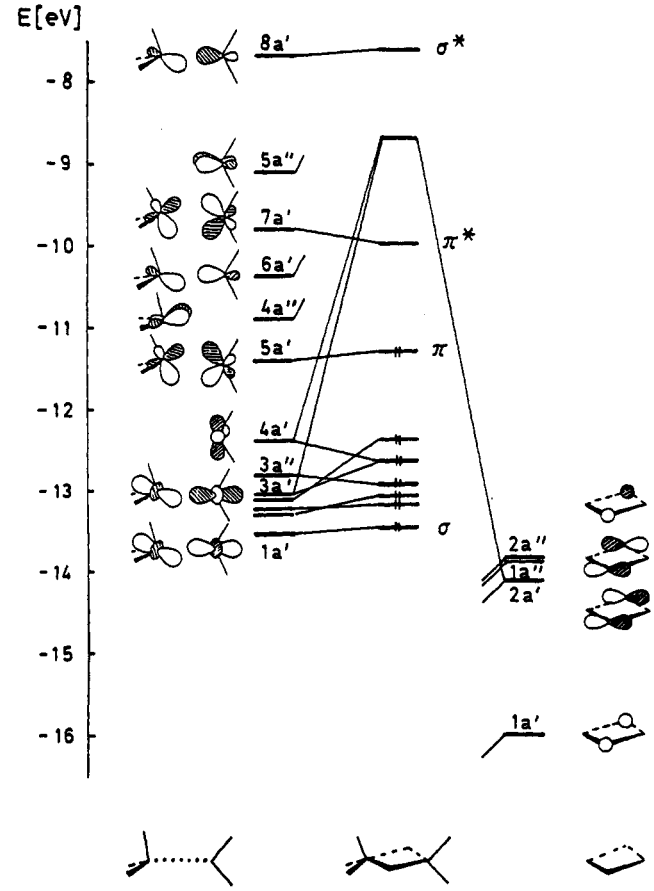

Figure 6. Molecular orbital diagram of $[Fe_2(CO)_5(\mu\text{-}PH_2)_2]$ built up from a $Fe_2(CO)_5$ fragment and two bridging coplanar PH_2 ligands.

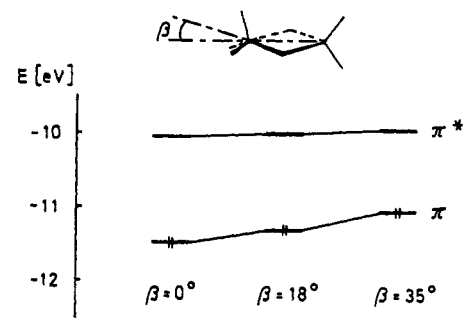

Figure 7. Energy variations of the bonding and antibonding Fe–Fe orbitals as a function of the angle β between the 3-fold axis of the $Fe(CO)_3$ fragment and the Fe–Fe bond axis.

analysis of the puckering in these species has already been described.[4i,20] Here we show in Figure 5 the important interactions between the $Fe_2(CO)_6$ fragment and the two bridging, noncoplanar, phosphido ligands. The higher orbitals $4a_1$, $2b_2$, $2a_2$, and $3b_1$ of the diiron fragment interact with the ligand orbitals a_1, b_2, a_2, and b_1, respectively. Essentially, the latter are combinations of σ and π lone pairs of the phosphorus atoms. In consequence, four Fe–P_{bridge} bonds are formed. Seven occupied orbitals remain in the frontier region. Six of these are the nonbonding d block (cf. "t_{2g}"); the HOMO is considered to indicate a "bent" Fe–Fe bond.[4c,21] Originally, the FMO $3a_1$ was an in-phase M–M bonding combination, but the geometric distortion of $(CO)_3M\cdots M(CO)_3$ toward a "sawhorse" changed the FMO character from π to bent σ.[22]

(18) Albright, T. A.; Burdett, J. K.; Whangbo, M.-H. *Orbital Interactions in Chemistry*; Wiley: New York, 1985.
(19) Summerville, R. H.; Hoffmann, R. *J. Am. Chem. Soc.* **1979**, *101*, 3821.
(20) Pinhas, A. R.; Hoffmann, R. *Inorg. Chem.* **1979**, *18*, 654.
(21) Anderson, E. L.; Fehlner, T. P.; Foti, A. E.; Salahub, D. R. *J. Am. Chem. Soc.* **1980**, *102*, 7422.

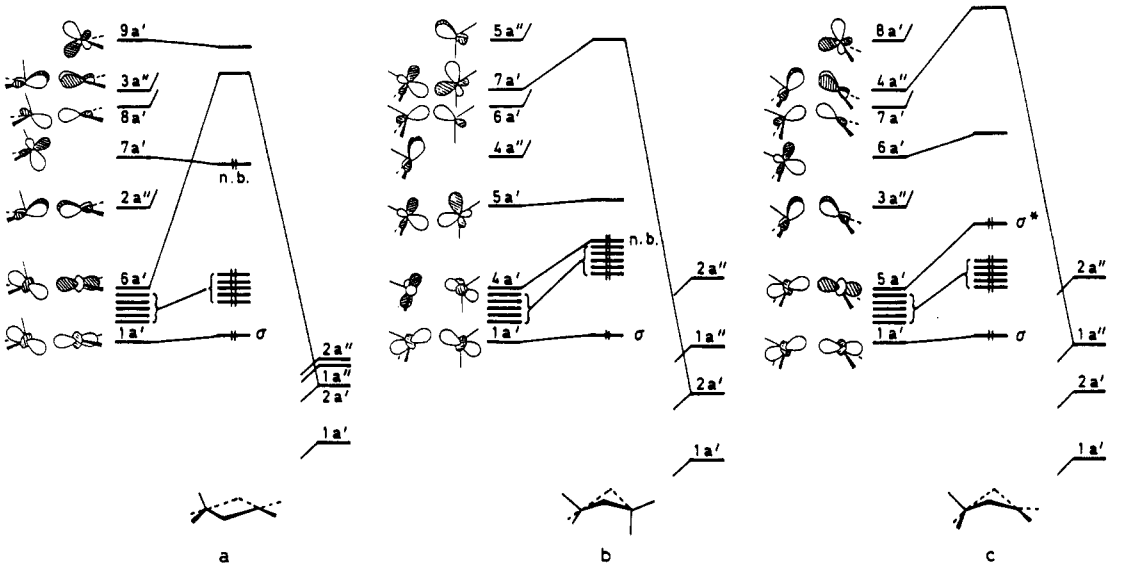

Figure 8. Diagrams for the interactions between the fragment Fe_2L_5 and two bridging PH_2 ligands in different geometrical arrangements: (a) planar Fe_2P_2 core and planar Fe1 coordination; (b) puckered Fe_2P_2 core and tetrahedral Fe1 coordination; (c) puckered Fe_2P_2 core and planar Fe1 coordination. Refer to Figures 4 and 5 for the orbital drawings of the relevant FMO's.

Figure 6 shows the calculated molecular orbital diagram for the model complex $[Fe_2(CO)_5(\mu\text{-}PH_2)_2]$ with a planar Fe_2P_2 core and distorted square-pyramidal coordination about the atom Fe2. As in the case of $[Fe_2(CO)_6(\mu\text{-}PR_2)_2]$, orbitals of the fragment $Fe_2(CO)_5$ mix with the phosphido donor orbitals to form the four metal–bridge bonds. Positive values of the overlap population between FMO's are calculated for the following interactions: 6a′ (on the left) interacts with 1a′ (right), 5a″ with 1a″, 4a″ with 2a″, and a mixture of 3a′ and 4a′ with 2a′. Notice that bonding and antibonding complex molecular orbitals arising from these metal–bridge interactions receive contributions from both iron atoms even if the $Fe_2(CO)_5$ fragment orbitals were originally localized on separate iron atoms and that the six lowest filled MO's are not all nonbonding. In fact, the level 3a′ is already engaged in Fe–P bonding. Moreover, the fragment orbital pairs 1a′/8a′ and 5a′/7a′ neither are part of the d block nor are they used for the metal–bridge bonds. The FMO's in question remain unchanged in the complex. Since 1a′ is filled and 8a′ is empty, this pair triggers the Fe–Fe σ bond, which is consistent with the interpretation of the bonding in the $Fe_2(CO)_9$ system.[23] In the present case we have a second pair of bonding/antibonding levels promoting a metal–metal bond. In conclusion, after the identification of all the interactions between metal atoms and bridging ligands, two two-electron/two-orbital interactions remain labeled σ/σ^* and π/π^* and represent the through-space Fe–Fe double bond expected by electron counting.

Quantitative evidence for the direct Fe–Fe bonds can be obtained by inspecting the overlap populations (OP) between the bond atoms (Table VII). If the levels descending from 1a′, 5a′, 7a′, and 8a′ identify the two pairs of Fe–Fe direct interactions, depopulation of either the σ orbital or the π orbital (which is easily possible in the framework of the EHMO method) should not change the OP_{Fe-P} values but should significantly lower the values of OP_{Fe-Fe}. Indeed, the metal–metal bonding character of both these orbitals is clearly indicated by the values in Table VII. Analogously, OP_{Fe-Fe} (but not OP_{Fe-P}) is reduced by occupation of the π^* orbital on account of the metal–metal antibonding character of this orbital. Finally,

Table VII. Overlap Population Values for the Complex $[Fe_2(CO)_5(\mu\text{-}PH_2)_2]$ with Depopulated Bonding and Antibonding Orbitals, Respectively

	OP_{Fe-Fe}	OP_{Fe2-P}	OP_{Fe1-P}
neutral complex	0.320	0.444	0.601
σ orbital empty	0.222	0.455	0.592
π orbital empty	0.210	0.442	0.596
π^* orbital filled	0.136	0.442	0.604

the artificial addition of two electrons into the second LUMO or in the higher orbital σ^* (see Figure 6) has the effect of reducing both the OP_{Fe-Fe} and OP_{Fe-P} values in both cases. Actually, the metal–metal and metal–bridge antibonding characters mix significantly in these levels. Nevertheless, these orbitals jointly play the role of the two Fe–Fe and Fe–P antibonding partners. From the FMO analysis it follows, however, that the orbital labeled σ^* is the major candidate to represent the Fe–Fe σ^* level of the system.

Following this, we analyzed the relationship between electronic structure and geometry in the complex $[Fe_2(CO)_5(\mu\text{-}PH_2)_2]$. First, the angle β between the 3-fold axis of the $Fe(CO)_3$ fragment and the Fe–Fe bond axis was varied. For all values of β the Fe–Fe double bond is essentially preserved (see Figure 7), although the π bond is most stabilized at low values of β (i.e. near the geometry used by us to build the interaction diagram of Figure 7). This is also reflected by the variations of the overlap population OP_{Fe-Fe}: $OP(\beta = 0°) = 0.342$, $OP(\beta = 18°) = 0.320$, $OP(\beta = 35°) = 0.278$. Thus, the electronic factors alone do not justify the experimentally observed coordination about the atom Fe2 (close to a square pyramid) in complexes **5** and **6**. Obviously, steric factors play a significant role in the stabilization of the system; the complex is only obtainable with bulky substituents at the phosphido bridges.

Additional calculations on $[Fe_2L_5(\mu\text{-}PH_2)_2]$ systems have been carried out to study the other geometrical features of these complexes, in particular relative to the coordination of atom Fe1. The orbital interaction diagram of Figure 8a would arise from planar rather than tetrahedral coordination of Fe1. The metal FMO that gave rise to the Fe–Fe π-bonding interaction (5a′ in Figure 5) is now primarily the "in-plane" FMO 2a″ that is involved in metal–bridge bonding. It interacts with the ligand orbital 2a″.

(22) Thorn, D. L.; Hoffmann, R. *Inorg. Chem.* **1978**, *17*, 126.
(23) Mealli, C.; Proserpio, D. M. *J. Organomet. Chem.* **1990**, *386*, 203.

Thus, the HOMO of the complex is now a nonbonding orbital strongly localized at the Fe2 atom. This leads to a reduced Fe–Fe overlap population value of only 0.162, compared to 0.310 for the tetrahedral case with the Fe–Fe double bond. The electronic picture in this case corresponds to that of an 18e five-coordinated iron atom (Fe2) coexisting with a 16e iron (Fe1). The stabilization of the latter is made possible by its square-planar coordination. In dimers of the type $[Rh_2(CO)_4(\mu\text{-}PR_2)_2]$, the progressive loss of Rh–Rh bonding due to the attainment of square-planar coordination at one or both metal atoms has been experimentally demonstrated and theoretically investigated.[24]

Another imaginable structure would be a puckered Fe_2P_2 core such as exists in the $[Fe_2(CO)_6(\mu\text{-}PR_2)_2]$ complexes. A schematic interaction diagram is shown in Figure 8b. Again, the metal–metal π-bond disappears (OP_{Fe-Fe} = 0.117). Due to the puckering, the orbital 5a′ remains essentially nonbonding, and it represents the LUMO of the system. Also, the orbital 4a′ does not interact with the ligand orbital 2a′. This, in turn, interacts better with the fragment orbital 7a′. Ultimately, 4a′ is a nonbonding orbital that belongs to the d block. The instability of this structure may be indicated by the small HOMO–LUMO gap. Indeed, the vacant 5a′ renders both metal atoms electronically unsaturated.

Finally, we consider a structure that has both a square-planar Fe1 atom and a puckered Fe_2P_2 core. From Figure 8c it can be seen that the HOMO is now a metal–metal σ-antibonding orbital; i.e. both the σ- and the π-bond vanish (OP_{Fe-Fe} = 0.052).

From this analysis it follows that a planar Fe_2P_2 core and a tetrahedral coordination about the atom Fe1 are required to form the iron–iron double bond expected by electron counting. Reduction of these complexes by adding two further electrons would lead to a species with a metal–metal single bond, since the newly occupied level is Fe–Fe π^* in nature. It is reasonable to assume that in this case the planar Fe_2P_2 core is retained. Experimental evidence is provided by the planar Co_2P_2 core structure of $[Co_2(CO)_5(\mu\text{-}PR_2)_2]$ (PR_2 = $\overline{PN(Me)CH_2CH_2N(Me)}$), which is electronically equivalent to the reduced form of these complexes.[25] The reaction chemistry of these unsaturated complexes is currently being investigated.

Structure and bond analyses of the unsaturated complexes **5** and **6** underline the influence of the number of the valence electrons on the core geometry of doubly phosphido-bridged carbonyl complexes. Dahl et al.[4j] showed that the butterfly-shaped complex $[Fe_2(CO)_6(\mu\text{-}PPh_2)_2]$ becomes planar upon reduction to the dianion because of loss of the metal–metal bond caused by occupation of the predominantly metal–metal antibonding LUMO. We show that loss of one 2e ligand, caused by steric requirements, likewise favors a geometrical change from a bent to a (nearly) planar Fe_2P_2 core, in this case, however, by formation of a double bond.

Lastly, the bond analysis given above for the unsaturated diiron complexes also supports a net metal–metal double bond for the isoelectronic bis(*tert*-butylphosphido)-bridged dicobalt complex as suggested by Jones et al.[5] on the basis of metal–metal bond length and electron count. The bond situation of the nickel complex $[Ni_2(CO)_3(\mu\text{-}PBu^t_2)_2]$,[6] on the other hand, remains questionable. It may either be an (18–16)e complex with a Ni–Ni single bond[6] or may have a comparable Ni–Ni double bond as suggested by the isoelectronic relationship.

Since the submission of this paper to the editor we became aware of a Ph.D. thesis by Adams[26] also containing the X-ray structure of complex **5**. These results have now appeared.[27]

Acknowledgment. We are grateful to Dr. G. Zahn (University of Leipzig) for X-ray intensity data collection and reduction for compounds **3** and **5** and Dr. Schneider (Halle) and Dr. von Löwis (Berlin) for running the UV/vis and the MS spectra, respectively.

Registry No. 1, 138899-31-7; 2, 138899-32-8; 3, 137868-81-6; 4, 138899-33-9; 5, 137868-80-5; 6, 138899-34-0; $Na[Fe_2(\mu\text{-}CO)(CO)_6(\mu\text{-}PPh_2)]$, 138899-35-1; $Na[Fe_2(\mu\text{-}CO)(CO)_6(\mu\text{-}PCy_2)]$, 138899-36-2; $Na[Fe_2(\mu\text{-}CO)(CO)_6(\mu\text{-}PMe_2)]$, 138899-37-3; $Na[Fe_2(\mu\text{-}CO)(CO)_6(\mu\text{-}PBu^t_2)]$, 138899-38-4; Ph_2PCl, 1079-66-9; Bu^t_2PCl, 13716-10-4; Cy_2PCl, 16523-54-9; $Fe_2(CO)_5(\mu\text{-}PH_2)_2$, 138899-39-5.

Supplementary Material Available: Listings of fractional coordinates and isotropic displacement parameters for H atoms, anisotropic displacement parameters for non-H atoms, and bond lengths and angles for **3**, **6**, and **5** (9 pages); F_o/F_c lists (67 pages). Ordering information is given on any current masthead page.

(24) Kang, S.-W.; Albright, T. A.; Wright, T. C.; Jones, R. A. *Organometallics* **1985**, *4*, 666.
(25) Hutchins, I. D.; Light, R. W.; Paine, R. T. *Inorg. Chem.* **1982**, *21*, 266.
(26) Adams, M. R. *Chem. Abstr.* **1991**, 220121c.
(27) Adams, M. R.; Gallucci, J.; Wojcicki, A. *Inorg. Chem.* **1991**, *31*, 2.